Computational Screening of Metal-Organic Frameworks for Biogas Purification

Journal:	*Molecular Systems Design & Engineering*
Manuscript ID	ME-ART-08-2019-000095.R1
Article Type:	Paper
Date Submitted by the Author:	21-Sep-2019
Complete List of Authors:	Demir, Hakan; University of Minnesota, Dept of Chemistry Cramer, Christopher; University of Minnesota, Department of Chemistry and Supercomputing Institute Siepmann, Joern Ilja; University of Minnesota, Dept of Chemistry

Design, System, Application

Metal-organic frameworks (MOFs) constitute a class of three-dimensional crystalline microporous materials that can offer large surface area and specific adsorption sites that makes them useful candidates for the energy-efficient adsorptive separation of gas mixtures, such as the biogas purification. Using a hierarchical screening process, we start from 5109 candidate MOFs, remove 1710 structures based on geometric criteria and type of metal node, use simulations for adsorption of binary mixtures CH_4/(CO_2 or N_2 or H_2S or NH_3) onto 3399 structures and simulations for five-component mixtures to find a potentially top-performing MOF structure based on selectivity, working capacity, and regenerability.

Computational Screening of Metal-Organic Frameworks for Biogas Purification

Hakan Demir[a], Christopher J. Cramer[a], and J. Ilja Siepmann[a,b,*]

[a] Department of Chemistry and Chemical Theory Center, University of Minnesota, 207 Pleasant Street Southeast, Minneapolis, MN 55455-0431, United States.

[b] Department of Chemical Engineering and Materials Science, University of Minnesota, 421 Washington Avenue Southeast, Minneapolis, MN 55455-0431, United States.

[*] E-mail: siepmann@umn.edu

Abstract

Biogas, which involves methane as the combustible compound, is an abundant and renewable energy resource that produces less harmful gases than conventional fossil-based liquid and solid energy sources. Although biogas is of primary interest due to its methane content, it may also include other gases, such as CO_2, N_2, H_2S, and NH_3. Studies investigating biogas purification often assume that biogas is a binary 50%/50% mixture of methane and carbon dioxide. However, together with N_2, the toxic contaminants, H_2S and NH_3 should be accounted for in the biogas mixture for a more realistic separation application. In this study, the computation-ready experimental metal-organic framework (CoRE-MOF) database is screened to identify a shortlist of potentially high-performing MOFs for multi-component biogas purification. Our hierarchical screening process involves (i) removal of MOFs with sub-3 Å pore limiting diameter and uncommon metal nodes, (ii) removal of MOFs that do not selectively capture the four undesired compounds, as determined from grand canonical Monte Carlo (GCMC) simulations for the binary mixtures of CH_4/(CO_2 or N_2 or H_2S or NH_3), and (iii) ranking of the remaining structures based on various performance metrics determined from GCMC for a five-component mixture. Finally, the relations between some of these metrics and structural properties are discussed to reveal favorable structural characteristics for biogas upgrading.

Design, System, Application

Metal-organic frameworks (MOFs) constitute a class of three-dimensional crystalline microporous materials that can offer large surface area and specific adsorption sites that makes them useful candidates for the energy-efficient adsorptive separation of gas mixtures, such as the biogas purification. Using a hierarchical screening process, we start from 5109 candidate MOFs, remove 1710 structures based on geometric criteria and type of metal node, use simulations for adsorption of binary mixtures CH_4/(CO_2 or N_2 or H_2S or NH_3) onto 3399 structures and simulations for five-component mixtures to find a potentially top-performing MOF structure based on selectivity, working capacity, and regenerability.

1 Introduction

Renewable energy sources have gained more importance as the consumption rate of fossil fuels has increased substantially since the industrial revolution. Biogas is one of the popular options in the renewable energy field since it can be produced in large quantities.[1] Biogas is generated from anaerobic degradation by microorganisms of biomass,[2–4] whose sources are landfills, industrial wastewater, household waste, animal waste, and crop residues. It is a multicomponent gas mixture produced at atmospheric pressure principally composed of CH_4 and CO_2, with many other contaminants such as N_2, NH_3, H_2S, H_2O, and others.[2,5] The composition of the biogas depends on the biomass source, however, typically, methane makes up about half to three quarters (by mole fraction) of the un-purified biogas while the remainder is dominated by CO_2 with some other contaminant gases.[6] Through combustion, biogas can be converted into heat or electricity. Biomethane derived from biogas can also be used in the biogas fuel cells and steam reforming of methane to generate hydrogen.[3] For all of these applications, biogas needs to be purified (95+% purity methane with only trace amounts of H_2S) before it can be transported by pipelines or stored in gas tanks.[7,8]

Compared to coal and petroleum, methane is a cleaner energy resource as its combustion results in less CO_2 per energy unit.[2,9] Obtaining pure methane from biogas (upgrading biogas) is a crucial target since the contaminants in the biogas do not only mitigate the heating value but also can lead to corrosion in the equipments and pipelines that are used to store/transport biogas.[9] For example, H_2S can pose corrosion threat to equipment since it can convert into corrosive and hazardous chemicals (i.e. SO_2, H_2SO_4).[7,10] In addition, H_2S is highly toxic and causes adverse health effects after prolonged exposure at concentrations above 10 ppm.[11] For fuel cell applications, removal of H_2S to 0.1 – 10 ppmv is critical.[10] NH_3 is also a toxic gas hazardous to human health and environment in small concentrations with a permitted exposure limit as low as 25 ppm.[12]

The biogas upgrading can help reduce the emissions of CO_2 and CH_4 into the atmosphere which are two of the principal sources for the greenhouse gas effect.[13] Although CH_4 emissions are lower than CO_2 emissions, CH_4 has much larger greenhouse warming potential than CO_2 per unit volume.[6,13–15] Also, separation of purified CO_2 from biogas would enable using it for various chemicals processes.[16] Today, many gas separations, including C_2H_6/CH_4[17], CH_4/N_2[17], CO_2/CH_4[18], are performed using cryogenic distillation, which is a very energy intensive process especially for low and medium scale separations.[19] There are several processes that are an alternative to cryogenic distillation, such as absorption, adsorption, and membrane separation.[4] Among these, adsorption can be an economical separation technique when an effective adsorbent is utilized for gas separation. Adsorption techniques, such as pressure swing adsorption (PSA) and vacuum swing adsorption (VSA), have drawn attention due to their relative ease of operation, and low investment cost.[13,20,21] Many previous studies assumed biogas to be a binary (50%/50%) mixture of CH_4 and CO_2 and material performances are tested accordingly. For example, zeolite 13X and 5A are used at such conditions and they are demonstrated to be effective materials for CO_2/CH_4 separation.[22,23] Santos et al.[24] have designed a two-column PSA process using zeolite 13X at T = 323 K and predicted that biogas can be effectively separated

with a methane purity of 99.2%. Jiang et al.[25] simulated the CO_2/CH_4 separation performance of zeolites NaUSY, APGI, LiX, and activated carbon using a VSA process for a biogas mixture of 50% CO_2, 50% CH_4 and ranked the best materials in the order of NaUSY > APGI > LiX > activated carbon. Using NaUSY, their process predicted to generate a methane stream with purity higher than 98% at 20 kPa vacuum pressure.

Compared to zeolites, metal-organic frameworks (MOFs) constitute a relatively new class of materials. They are nanoporous, crystalline structures that have attracted immense attention especially in the last two decades due to their advantageous structural features, namely high surface area, pore volume, chemical versatility, and functionalization opportunities.[26–28] As the name implies, MOFs are principally composed of two moieties, a metal node and an organic linker. Since there are many possible metal nodes, organic linkers, and network topologies, the number of MOF structures that can be formed through different combinations of these two building blocks is almost limitless.[29] The numbers of MOFs synthesized or predicted by computational means are growing rapidly, and there are several MOF databases collecting large number of structures.[29–31] Many experimental and theoretical studies have explored MOFs for gas storage, gas- and liquid-phase separations[32–34], catalysis[35–37], and sensing.[38,39] There have been many experimental and theoretical studies relevant to biogas upgrading some of which are outlined below.

Pal et al.[40] examined the $CO_2/CH_4/N_2$ separation performance of a Co-MOF, IITKGP-6, by measuring adsorption isotherms and observed the strength of gas affinity in the order of CO_2 > CH_4 > N_2. Using ideal adsorbed solution theory (IAST)[41], they determined high CO_2/N_2 (15% / 85 % bulk gas composition) and CO_2/CH_4 (50% / 50 % bulk gas composition) selectivities of 51 and 36, respectively, at T = 273 K and P = 100 kPa. Cavenati et al.[42] measured CO_2 and CH_4 uptake in Cu-BTC at T = 303, 323, and 373 K and determined a CO_2/CH_4 selectivity in the range of 4-6 at T = 303 K and for P = 0-4 bar, where the selectivity was found to decrease as the pressure increases. They suggested Cu-BTC as an adsorbent for a VSA process to upgrade biogas. Ferreira et al.[43] investigated the purification of methane using MIL-53 (Al) and determined a CO_2/CH_4 selectivity of 4.1 at T = 303 K for the pressure range of 0.1 – 3.5 bar through fixed-bed experiments suggesting it be used in a PSA process. Their designed PSA process for biogas upgrading predicts CH_4 and CO_2 purities as 99.4% and 95.4%, respectively.

Xiang et al.[16] studied the separation performance of UTSA-16 for CO_2/CH_4 (50% / 50%) under ambient conditions. Their IAST[41] calculations showed that UTSA-16 can perform better than many other materials reported in the literature including Cu-BTC, MIL-101, MFI, in terms of CO_2/CH_4 selectivity, however, they predict lower selectivity for UTSA-16 compared to JBW, Mg-MOF-74, and NaX. Nugent et al.[44] reported the CO_2/CH_4 selectivities (using IAST) at T = 298 K and P = 1 bar of 5.3, 33, and 231 for SIFSIX-2-Cu, SIFSIX-2-Cu-i, and SIFSIX-3-Zn, respectively, where the latter selectivity is higher than CO_2/CH_4 IAST selectivity for Mg-MOF-74 (137), and zeolite 13X (103).[44]

Wilmer et al.[45] screened more than 130,000 hypothetical MOFs to investigate CO_2/CH_4 (50% / 50%) separation using grand canonical Monte Carlo (GCMC) simulations at T = 298 K and various pressures for three different scenarios, namely natural gas purification with PSA, landfill

gas separation with either PSA or VSA. For the separation of landfill gas using VSA, they found that MOFs with small pores and high CO_2 heat of adsorption are ideal while carrying out the same separation using PSA would favor larger pore sizes. Alsmail et al.[46] studied the CO_2 and CH_4 adsorption characteristics of a Cu-MOF, NOTT-125a, both experimentally and theoretically. Using a customized force field for the framework to describe CO_2 adsorption, the GCMC simulations predicted excellent corroboration with experimental data. Similarly, describing the framework atoms with the DREIDING force field, the simulations yielded excellent agreement with the experimental data for CH_4 adsorption. NOTT-125a offers a satisfactory CO_2/CH_4 selectivity of 9.2 at T = 273 K and of 4.8 at 298 K. Zhang et al.[47] studied CO_2, N_2 and CH_4 adsorption/separation in Cu-TDPAT using GCMC simulations where the framework atoms were described by a combination of OPLS-AA and UFF parameters. Their GCMC simulations for binary mixtures (CO_2/CH_4 and CO_2/N_2) showed good agreement with IAST predictions which anticipate CO_2/CH_4 and CO_2/N_2 selectivities of 15-30 and 80-120, respectively, at T = 298 K in the pressure range of 0-1 atm for 50%/50% bulk gases. Borges et al.[48] utilized generic force fields in GCMC simulations to determine the CO_2/CH_4 and CO_2/N_2 separation performance of MIL-160. Firstly, they computed the single-component adsorption isotherm for CO_2, CH_4, and N_2 at T = 303 K and observed good agreement of GCMC predictions with the experiments. Simulating the separation of binary mixtures of CO_2/CH_4 (50%/50%) and CO_2/N_2 (15%/85%) at P = 1 bar, strong preferences for CO_2 over CH_4 and N_2 were found with CO_2/CH_4 and CO_2/N_2 selectivities of 10 and 35, respectively. By performing coadsorption experiments at relevant conditions, they determined similar selectivities as the GCMC predictions. Bae et al.[49] simulated CO_2 and CH_4 adsorption at T = 296 K in $Zn_2(NDC)_2(DPNI)$ using GCMC with generic force field parameters. Their binary GCMC simulations showed the CO_2/CH_4 selectivity to be in the range of 6-15 for the pressure range of 0-20 bar.

In this work, we use binary and five-component GCMC simulations to evaluate the performance of the structures in the computation-ready experimental metal-organic framework (CoRE-MOF) database for biogas separation using a VSA process. Recently, adsorption of binary and four- and five-component mixtures was used to assess the performance of zeolites for natural gas sweetening[50,51]. The current study utilizes a three-step hierarchical screening process involving an initial selection of CoRE MOFs based on the pore-limiting diameter and type of metal node, followed by evaluation of the performance for binary gas mixtures, and culminating in five-component (50% CH_4, 45% CO_2, 3% N_2, 1% H_2S, and 1% NH_3) GCMC simulations to identify high-performing MOFs for biogas upgrading using more realistic gas mixture conditions.

2 Computational methods

The CoRE-MOF database 2014 includes 5,109 structures.[31] To designate the operations performed on the experimentally determined structures during the process used to achieve input structures for molecular simulations, Chung et al.[31] have added suffixes to the reference codes of the CoRE MOFs. The suffixes appearing in our list of materials are explained as follows: “clean”

is utilized for structures where both free and bound solvent molecules are removed from the experimentally determined crystal structure; "manual" denotes manual modification performed for non-ionic species; "ion_b" is a label for ion-involving structures which have been manually modified; "charged" designates structures where besides the connected framework, the algorithm detects charged ionic species as separate molecules. The full list of these suffixes are available in the Supporting Information of Chung et al.[31]

The porous domains of these structures are characterized by several structural features such as the pore limiting diameter (PLD), the largest cavity diameter (LCD), the global cavity diameter (GCD), surface area, and probe occupiable pore volume. PLD defines the maximum size of a sphere that can percolate through a structure without overlapping any framework atoms.[52,53] LCD is the biggest pore opening along the percolating pore network.[52] GCD is the largest cavity that can be located in the framework.[54] Note that for a structure with multiple porous domains, GCD and LCD can be of different sizes.[55] The surface area and probe occupiable pore volume of a porous structure is determined by using Monte Carlo sampling as described in more detail in the literature.[56,57] All of these structural features are obtained by the Zeo++ code[56] using a probe diameter of 3.0 Å, where Zeo++ creates a graph representation of the porous space using Voronoi network to acquire pore characteristics.

To eliminate MOFs where diffusional limitations are highly expected, only CoRE MOFs that possess a pore limiting diameter (PLD) larger than 3 Å are selected. Although the kinetic diameter of CH_4, the largest of the five components, is 3.8 Å, a more conservative value is used for this initial screen to account for the flexibility of MOFs. We find 4162 MOFs with PLD > 3 Å. MOFs containing atom types that do not have sufficient ionization potential or electron affinity data in the EQeq code[58] are also discarded (759 structures of the 4162 MOFs passing the first screening step). Four additional MOFs (JACQUA_charged, SETTAO_clean, SENWEP_clean, and XACYAB_clean) structures are excluded as well since some of the atoms in those structures are too close to each other. Thus, in the first step of the screening, 1710 structures (33%) are eliminated.

In the second step, the remaining 3399 CoRE MOF structures are screened based on selectivity for four binary mixtures (CH_4/N_2, CH_4/CO_2, CH_4/H_2S, and CH_4/NH_3) using an equimolar composition at T = 298 K and P = 1 bar. To this extent, we carry out short GCMC simulations consisting of a total of 5,000 cycles (where 1 cycle = max (20, N) Monte Carlo steps with N being the maximum number of adsorbed molecules) that are split equally into equilibration and production periods. The adsorption results from this initial screening are collected, and 153 MOF structures that are selective towards all four contaminants (i.e., $S_{X/CH_4} > 1$ where X = N_2, CO_2, H_2S, and NH_3) over methane, are chosen for the third screening stage. It is noteworthy that by following our hierarchical screening approach, it has been made possible to downsize the list of materials to only 3% of the initial list which is subsequently employed in the computationally most demanding stage of our screening study, five-component GCMC simulations, as discussed below.

In the third screening stage, GCMC simulations for these 153 structures are carried out using a five-component gas mixture (50% CH_4, 45% CO_2, 3% N_2, 1% H_2S, and 1% NH_3) at T = 298 K

and adsorption and desorption pressures of 1 and 0.1 bar, respectively. Applying the same composition for adsorption and desorption corresponds to utilizing an infinite amount of feed gas. This is a simplification that streamlines the workflow and greatly reduces computational cost, but other computational studies have considered the desorption process in more detail[59]. These GCMC simulations are run for a total of 60,000 cycles separated into 10,000 equilibration and 50,000 production periods. For 9 MOFs (COYTIU_clean, DAPXID_ion_b, EGELUY01_manual, GUPJEG01_clean, JOSNAG_clean, JOSNAG01_clean, MEJZIM_clean, NISBEX_clean, and SAKNOJ_clean), the simulation cycles have been doubled to reduce the statistical uncertainties in the adsorbate loadings. It has been observed that in many MOFs either CO_2 or NH_3 dominantly adsorbs over other gas molecules resulting in poor statistics for the weakly adsorbing species. Out of 153 MOFs, only 40 MOFs are analyzed in detail because the relative standard deviations for CH_4, CO_2, H_2S, and NH_3 loadings are less than 10%, whereas the standard deviations are larger for N_2 because it does not adsorb in sufficient amounts. The computational resources required for the 153 longer GCMC simulations for the five-component gas mixture is about 20% of the resources required for the 13596 shorter GCMC simulations for binary mixtures; that is, using the hierarchical screening approach requires a significantly smaller effort.

The GCMC simulations utilize the RASPA software.[60] Translation, rotation, insertion/deletion, reinsertion (where an existing adsorbate molecule is reinserted independent of its current location in the framework), and molecule identity exchange moves are allowed with equal probability. The chemical potential values for the gas molecules are calculated using the Peng-Robinson equation of state with parameters from experimental values of the critical temperature, critical pressure, and acentric factor.[60] The unit cells of the MOFs are replicated to yield a supercell for the simulations that is sufficiently large to encompass a sphere with a diameter of 24 Å. Sorbate-sorbate and sorbate-framework interactions are described through Lennard-Jones (LJ) potential with a spherical potential truncation at 12 Å without tail-correction and the Coulomb potential using Ewald summation with 10^{-6} relative precision. The partial charges for the MOF atoms are determined using the EQeq method and framework atom LJ parameters are taken from the universal force field (UFF)[61]. EQeq is a semi-empirical charge equilibration method derived to estimate partial charges of atoms using ad hoc parameters.[58] As it does not require electronic structure calculations, the partial charges can be estimated swiftly. The TraPPE models are used for CH_4,[62] N_2,[63] CO_2,[63] H_2S,[64] and NH_3.[65] Throughout the GCMC simulations, the framework atom positions are kept fixed because specialized force fields are needed to govern framework motion (that are not available for the overwhelming majority of the 3399 structures used in simulations) and sampling these vibrational degrees of freedom adds significantly to the computational expense.

The performance of the MOFs is evaluated using several metrics, namely gas uptake at adsorption conditions (Q^{ads} in units of mol/kg), selectivity (S), working capacity (ΔQ in units of mol/kg), and regenerability (R). Selectivity is a metric to assess how effective the separation is, which is defined as

$$S_{12} = \frac{x_1}{x_2} / \frac{y_1}{y_2} \quad (1)$$

where x_1 denotes the adsorbed number of molecules of species 1 per unit cell at the adsorption pressure, and y_1 is the mole fraction of species 1 in the bulk gas phase. Working capacity is the amount of gas that can be removed from the material in the VSA process and it is calculated as

$$\Delta Q_1 = Q_1^{\text{ads}} - Q_1^{\text{des}} \quad (2)$$

where Q_1^{des} is the adsorbed gas amount of species 1 at the desorption pressure. Regenerability denotes the percentage of gas that can be recovered from the material during a VSA cycle and is determined as

$$R = \frac{\Delta Q_1}{Q_1^{\text{ads}}} \times 100 \quad (3)$$

Kohn-Sham density functional theory (DFT) optimizations are carried out in the Vienna Ab Initio Simulation Package (VASP[66,67]) using PBE-D3 (BJ).[68–70] These calculations employ 500 eV kinetic energy cutoff using Γ-point sampling. During the optimizations, only atomic positions are relaxed with the energy and force convergence criteria of 10^{-5} eV and 0.03 eV/Å, respectively.

3 Results and discussion

Since the aim of biogas separation is obtaining methane to be used in various applications, ideally, the adsorbent(s) should be able to separate all contaminants from methane. To reduce the separation cost, it would be preferred to have a single material that can purify methane in a single stage rather than using multiple adsorbents in multiple stages. Also, a good adsorbent should possess a high working capacity and regenerability for efficient separation. In this work, the feasibility of CoRE MOFs for efficient biogas upgrading is investigated using GCMC simulations at two levels.

The binary selectivities for equimolar mixtures of CO_2/CH_4, N_2/CH_4, H_2S/CH_4, and NH_3/CH_4 are depicted in Figure 1. Materials that do not adsorb any CH_4 molecules have infinite selectivity by definition and they are not plotted, but are included in the set of promising materials. Most of the CoRE MOFs are predicted to have a modest CO_2/CH_4 selectivity of 1-10, but there are some MOFs that exhibit very high selectivity (> 10^3). A large fraction of the CoRE MOF structures contains undercoordinated metal sites that can act as strong and specific adsorption sites for specific guest molecules. However, it is well understood that the UFF force field does not capture these specific interactions and tailored force fields or more expensive approaches to treat the interactions are required.[71–74] Selectivities for CO_2 over CH_4 greater than 10^3 are not

expected to arise solely because of favorable first-order electrostatic interactions of CO_2 with the framework but are likely more attributable to size exclusion of the larger-diameter CH_4 molecule. The LJ diameter of the united-atom methane model is 3.73 Å compared to a value of only 3.05 Å for the oxygen site in the CO_2 model. It has been reported earlier[75] that, generally, N_2 uptake of materials is lower than CH_4 and most of the CoRE MOFs are found to behave similarly in the binary GCMC calculations with a N_2/CH_4 selectivity in the range 0.1-1 is observed with the highest frequency. As can be seen in Figure 1, only a minor fraction of CoRE MOFs prefers N_2 over CH_4. Again, size exclusion (the LJ diameter of the nitrogen site in the N_2 model is 3.31 Å) is likely the reason for any MOF yielding N_2/CH_4 selectivity greater than unity when the simulations are carried out with molecular mechanics force fields. For the H_2S separation from CH_4, all the MOFs investigated here are found to be selective towards H_2S, and H_2S/CH_4 selectivities in the range of 10-100 are most prevalent. The TraPPE H_2S model includes LJ sites on sulfur and hydrogen atoms, but the combined size in the two directions perpendicular to its dipole vector is similar to CH_4; thus, inverse selectivity due to methane's size is not observed. The NH_3/CH_4 selectivity varies by several orders of magnitude depending on the MOF and, dominantly, it is predicted to be between 1 and 100. The LJ diameter and well depth of the N site in the NH_3 model are 8% smaller and 25% larger than those of CH_4, and size exclusion likely plays a large role for any of the more extreme selectivities ($> 10^3$).

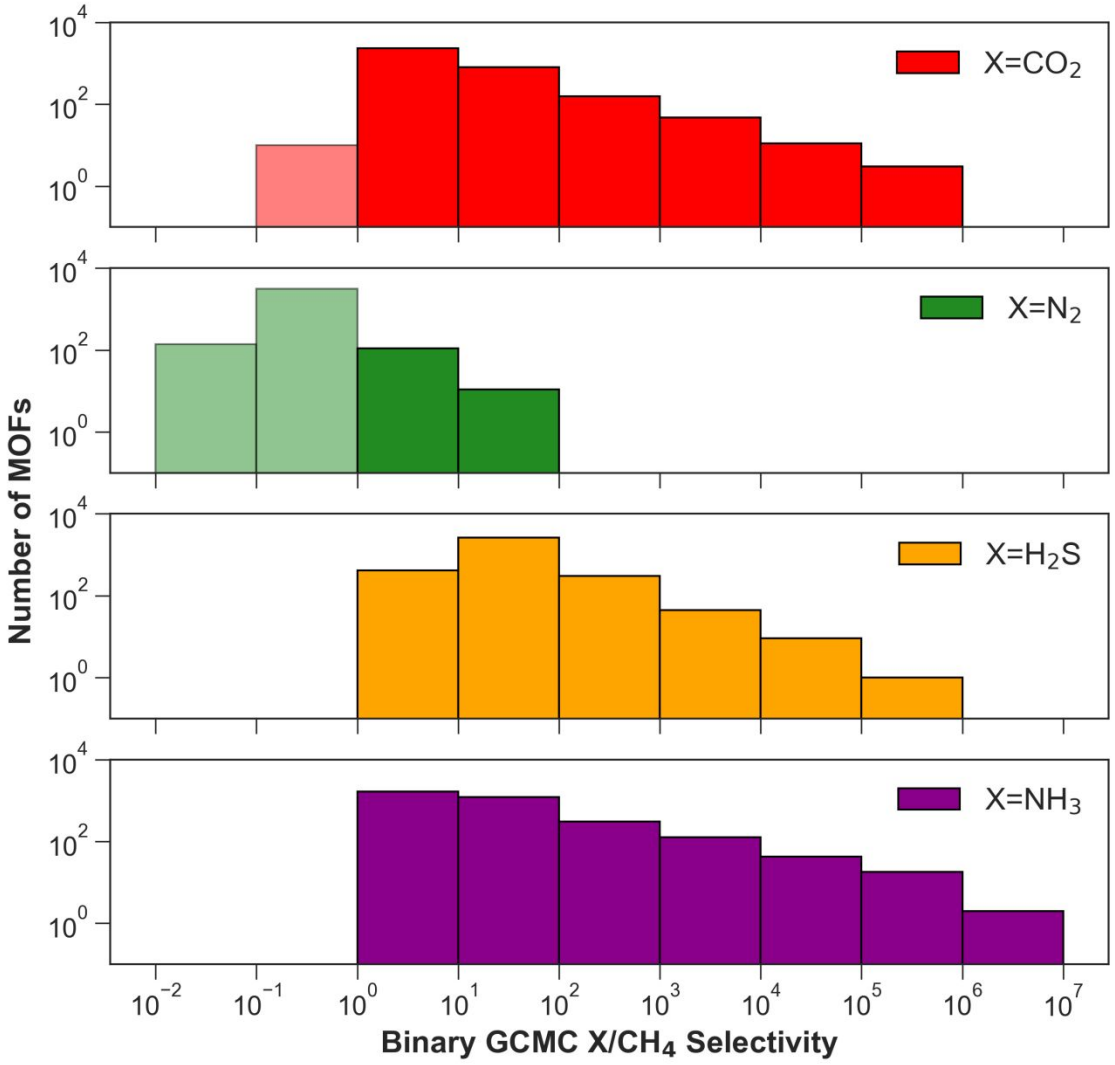

Figure 1. Distributions of selectivities for contaminants over methane calculated from binary GCMC simulations for equimolar mixtures.

The screening approach is based on working on a smaller but promising subset of MOFs in the more realistic five-component biogas mixture based on the binary GCMC data. These more complex simulations allow incorporating the effects of competitive adsorption of all gases that is absent in the binary GCMC simulations typically done for biogas upgrading. To this end, 153 MOFs which show preferential adsorption for contaminants (selectivity larger than 1 for each of the four contaminants) in the binary GCMC simulations are selected for the five-component GCMC simulations where the sorbate loadings are calculated both at 0.1 bar (desorption pressure) and 1 bar (adsorption pressure) at T = 298 K. In Figure 2, selectivity data obtained from the five-component GCMC simulations are plotted with respect to working capacity and colored according to regenerability, where each circle represents one of the 40 MOFs for which loadings with sufficient precision could be obtained for all five components. Numerical values

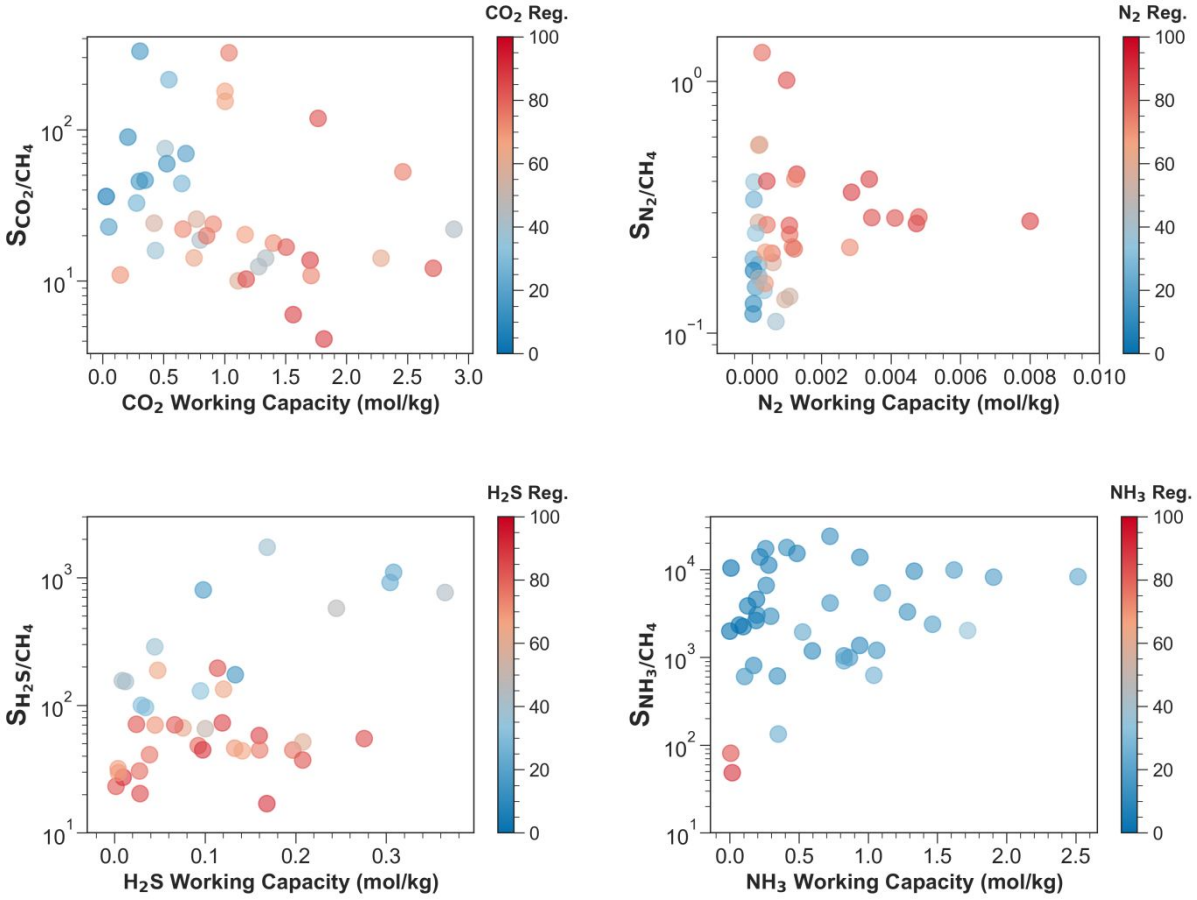

Figure 2. The correlation between selectivity, working capacity, and regenerability.

are provided in Tables S1-S3 in the Supporting Information. (As visual examples, adsorption loadings from binary and five-component GCMC simulations are shown for four MOFs in Figures S1 and S2.). For the CO_2/CH_4 separation, there are MOFs which can highly selectively capture CO_2 over CH_4 (i.e., selectivity > 10^2) with a large range of CO_2 regenerability and working capacity. In a typical selectivity versus working capacity plot, the best materials would ideally stand near the upper-right corner. For CO_2 separation from biogas, there are CoRE MOFs which can have high working capacity (i.e. 2 mol/kg) with a modest CO_2/CH_4 selectivity (10 to 100). Likewise, if selectivity is considered more significant for a particular application, a CoRE MOF with a selectivity of 100 to 300 can be selected that would have CO_2 working capacity around 1 to 1.8 mol/kg with medium-high regenerability (66-84%). However, we do not observe any material that exhibits both high working capacity (>2 mol/kg) and selectivity (>10^2) for CO_2. Because of the competitive adsorption that N_2 experiences with the strongly adsorbed components, it can be seen that N_2 working capacities are very low (practically zero) and all but two structures (GUPJEG0_clean and IRISAD01_charged) yield N_2/CH_4 selectivities less than 1. Thus, none of the MOFs can effectively capture N_2 from the simulated five-component gas mixture. This shows the importance of using realistic gas mixtures rather than binary gas

mixtures where N_2 is able to adsorb into smaller pores not accessible to CH_4 but gets displaced by the stronger adsorbing CO_2 and NH_3 molecules that can also access these smaller pores. In comparison to N_2, H_2S working capacities are larger (up to ~0.4 mol/kg). However, many of the highly selective (>10^2) MOFs have small working capacities (<0.1 mol/kg) showing the compromise between selectivity and working capacity. The best MOFs in terms of both high selectivity and high working capacity are EGELUY01_manual, QONQEQ_manual, and ARUYES_clean with H_2S/CH_4 selectivities of 1100, 920, and 760, respectively, and H_2S working capacities of 0.31, 0.30, and 0.36 mol/kg, respectively. However, these MOFs have relatively low H_2S regenerability values of 22, 24, and 43%, respectively. This trade-off is expected because high selectivity requires very favorable adsorption sites, but desorption from these sites requires very low pressure. For selective NH_3 capture, there are MOFs with very large NH_3/CH_4 selectivity (>10^3) with NH_3 working capacities typically less than 2.6 mol/kg. The drawback of these MOFs is their very low NH_3 regenerability, mostly less than 20%. On the other hand, MOFs that can provide high NH_3 regenerability (>75%) show considerably lower NH_3/CH_4 selectivity (<10^2). Among all MOFs, the three highest NH_3 working capacities (2.5, 1.9, and 1.7 mol/kg) belong to ZUQVOW_charged, QONQEQ_manual, and GIQYEL_clean, respectively.

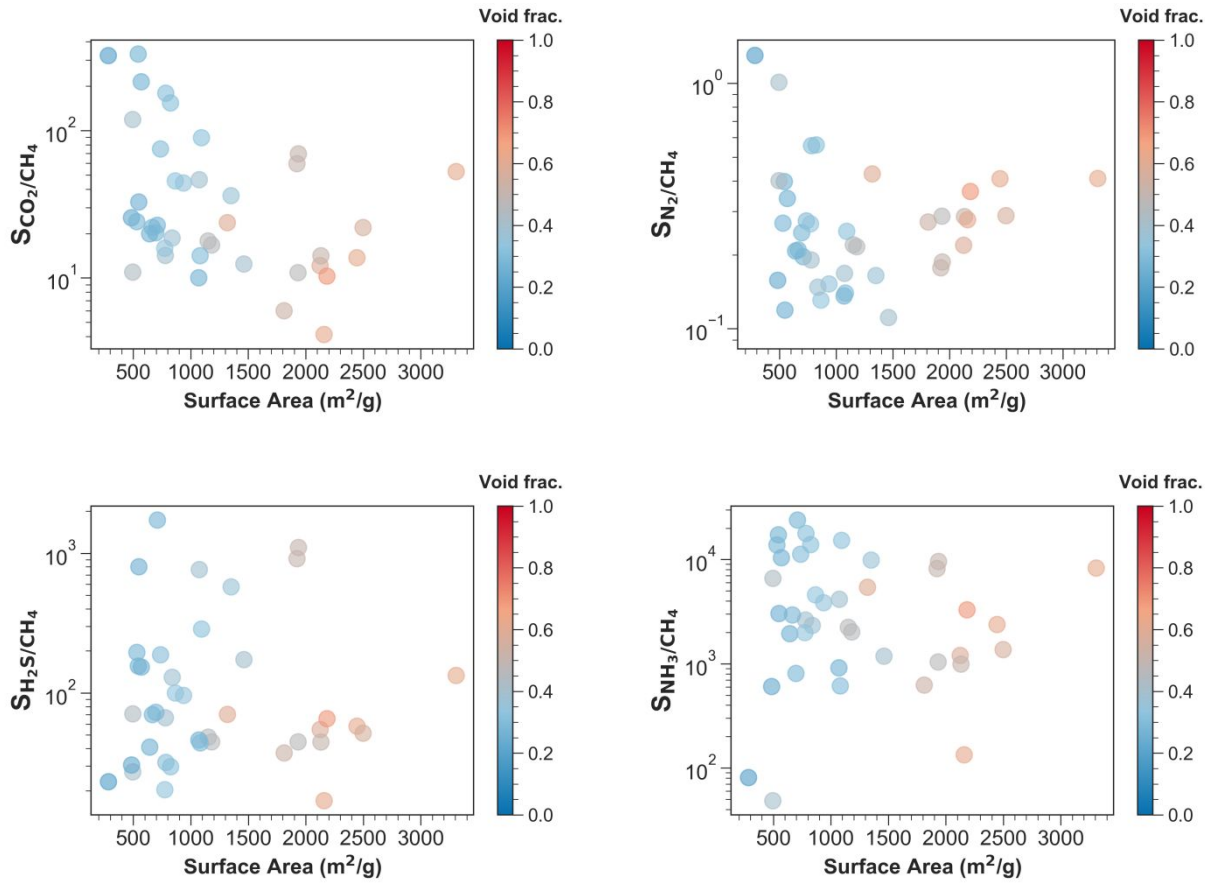

Figure 3. The correlation between selectivity, surface area, and void fraction.

In Figure 3, the selectivity data are plotted as function of surface area and colored according to void fraction. Numerical values for the pore characterization are provided in Table S4. MOFs that have very high CO_2/CH_4 selectivity (>10^2) have relatively low void fractions (0.18-0.40). Concomitantly with their low void fractions, these MOFs possess low surface areas (284-825 m^2/g) which is not favorable for separation performance. MOF surface areas of the selective structures are mostly less than 1000 m^2/g while there are selective MOFs which have larger surface areas (>2000 m^2/g). It can also be seen that N_2 selective MOFs have very low surface areas (<500 m^2/g) which is another reason indicating that MOFs without special consideration for dative bonding to open metal sites[76] may not be effective at separating N_2 from biogas. Most of the H_2S selective MOFs possess medium surface areas around 1000 m^2/g while one MOF (ZUQVOW_charged) is found that is both highly H_2S selective and have high surface area (selectivity >10^2, surface area 3308 m^2/g). Similar to CO_2, many MOFs can have very high NH_3/CH_4 selectivity, but the correlation with surface are is weaker in this case than for the CO_2/CH_4 selectivity. Some MOFs possess both high NH_3/CH_4 selectivity (10^3 - 10^4) and high surface area (>2000 m^2/g).

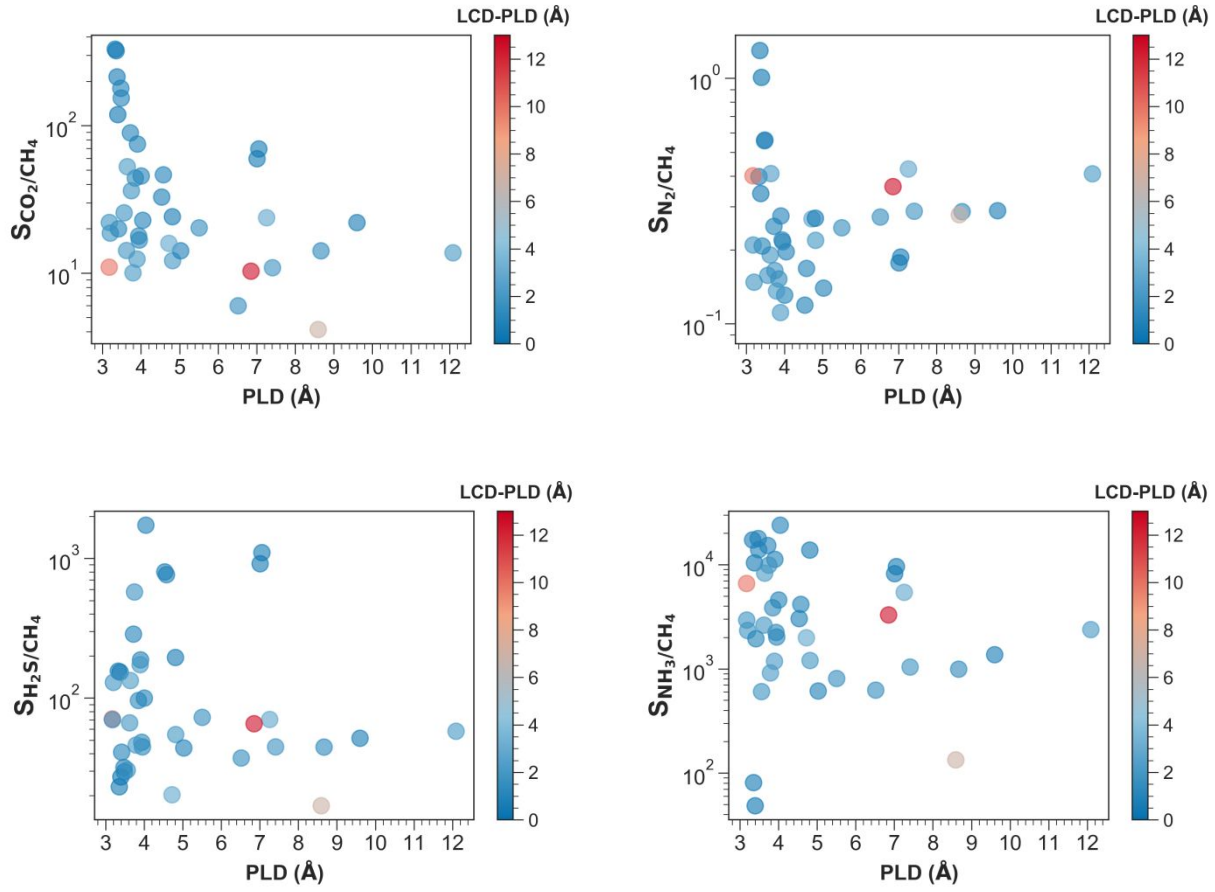

Figure 4. The correlation between selectivity and pore characteristics: PLD and pore bumpiness (= LCD − PLD).

One of the crucial properties of microporous structures is the PLD provides information about likely diffusional constraints. In Figure 4, the relation between selectivity, PLD, and pore bumpiness[77] is depicted. One important factor that Figure 4 reveals is that MOFs that possess high CO_2/CH_4 selectivity have a very narrow PLD (<4 Å) that leads to selectivity via size exclusion. Around PLD values of 3-4 Å, the CO_2/CH_4 selectivity drops drastically. Clearly, molecular sieving plays an important role for the biogas mixture as highly selective materials generally have a low PLD and a small LCD-PLD difference. A similar behavior is seen for N_2/CH_4 selectivity around 3 - 4 Å. For the H_2S/CH_4 separation, MOFs with small pores can have highly varying performance where selectivity can be between 20 - 2×10^3, but H_2S is most similar in size to CH_4 and sieving is not expected to play a significant role for this pair. Similar performance variance can be seen for NH_3/CH_4 separation at low values of the PLD.

Although we do not find any MOF that can simultaneously capture all contaminants effectively due to the low N_2 selectivity and working capacity, there are MOFs that can separate multiple species from a multi-component mixture of biogas with high selectivity. It should be noted that N_2 is vastly more benign than the other three contaminants, but the low critical temperatures of CH_4 and N_2 lead to a high energy demand for cryogenic distillation. To identify potentially high-performing structures for the biogas purification, the following criteria have been chosen to rank the 40 MOFs: (i) by the product of the selectivities for CO_2, H_2S, and NH_3 over CH_4 where the unweighted product reflects the higher toxicity of H_2S and NH_3, (ii) by the weighted sum of working capacities, i.e., $10\times WC_{CO2} + WC_{H2S} + WC_{NH3}$ where the weighted sum accounts for the larger amount of CO_2 that needs to be removed; and (iii) by the sum of the regenerability rankings (except for N_2) following the first-place convention (see Tables S5-S7 for the ranked lists).

Figure 5 shows a Venn diagram for the top-20 CoRE MOFs found using each of the three criteria. It should be noted that HEDBEZ_clean, and PEJMOI_clean do not make it into any of the three top-20 MOF lists, while the other 38 MOFs are found in at least one of those lists. ZUQVOW_charged, WASTUG_clean, and JOSNAG_clean are the three MOFs that are present in all three top-20 CoRE MOF lists. There are 3 (12) common CoRE MOFs that have high performance based on the regenerability rankings and the product of the selectivities (working capacity criterion) but not working capacity criterion (the product of the selectivities). Similarly, 1 CoRE MOF is found that performs well based on the intersection of selectivity and working capacity criteria excluding the regenerability criterion. Lastly, there are 13/4/2 top CoRE MOFs identified using selectivity/working capacity/regenerability criterion that are not found in other lists of top performing materials.

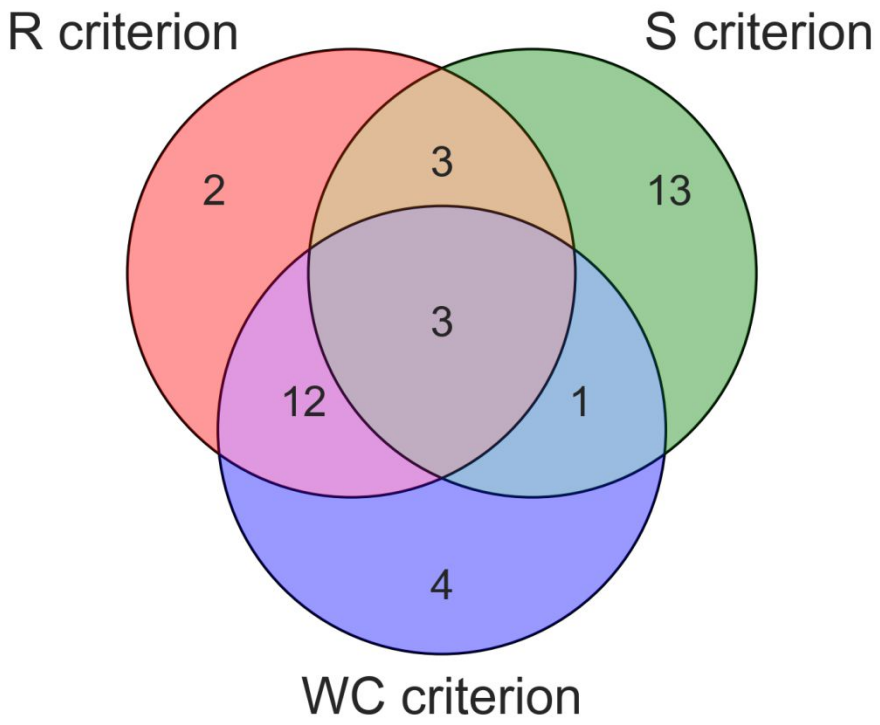

Figure 5. Venn diagram showing the 20 high-performing CoRE MOFs selected based on three criteria: selectivity (product of three selectivities), working capacity (weighted sum of three working capacities), and regenerability (sum of three regenerability rankings).

The selected top-3 MOFs (ZUQVOW_charged, WASTUG_clean, and JOSNAG_clean) have high selectivities and moderately high working capacities. However, as it can be noticed from Table S3, their main shortcoming is the relatively low regenerability for NH_3. Low regenerability results from the loading at the adsorption pressure falling outside of the linear Henry's law regime (i.e., being near saturation of the strong adsorption sites where a decrease in partial pressure by a given factor is not accompanied by a similar decrease in the loading).

Since the CoRE-MOF database is prepared by batch processing experimentally reported structures through structure cleaning codes, there could be cases where the cleaning procedure might be too aggressive resulting in unstable structures. To evaluate the reliability of the cleaning procedures for the top-performing CoRE MOFs, we check for agreement of the MOF composition and mechanical stability of the unit cell via optimization using periodic DFT calculations. First, the structural formulas of CoRE MOFs are compared with their experimentally reported counterparts. For the ZUQVOW_charged structure, it is found that the cleaning procedure leads to PF_8 moieties rather than the PF_6 units observed experimentally. This

change in the chemical formula suggest a problem with the automated cleaning process; thus, its DFT optimization is not attempted. The experimentally reported WASTUG structure lacks hydrogens on bridging oxygens which were not added during the cleaning process for the CoRE-MOF database, preventing charge neutrality. Therefore, the WASTUG_clean structure is also not suitable for DFT optimizations. On the other hand, the difference between the chemical formula of the unit cell in the CoRE-MOF database and that observed experimentally for JOSNAG ($\{[La_2(ad)_3(H_2O)_4]\cdot 6H_2O\}_n$, ad = adipato; $C_6H_8O_4^{2-}$) is the hydration water molecules. DFT optimization is performed for JOSNAG_clean assuming singlet spin state. As can be seen from the data in Table 1, the optimized JOSNAG_clean structure has slightly (by about 3%) contracted pore diameters resulting in 9% smaller pore volume and void fraction compared to the unoptimized JOSNAG_clean structure. However, the surface area is reduced by 16% indicating a smoothening of the pore walls. Although diffusional properties are not in the scope of this study, for an actual gas separation process, diffusional limitations can play a significant role. Due to the small pore sizes in the JOSNAG_clean structure, diffusional limitations may arise for some of the undesired components of the biogas mixture (CO_2, N_2, and H_2S).

Table 1. Properties of pore space of top two MOFs

MOF	GCD (Å)	PLD (Å)	LCD (Å)	Surface Area (m^2/g)	Void Fraction	Pore Volume (cm^3/g)
Initial JOSNAG_clean	4.32	3.48	4.27	783.6	0.308	0.206
Optimized JOSNAG_clean	4.25	3.30	4.20	676.8	0.283	0.189

GCD = Global Cavity Diameter, PLD = Pore Limiting Diameter, LCD = Largest Cavity Diameter

We note that JOSNAG contains La as metal node. The EQeq method predicts partial charges of these La nodes as 1.936 |e| for JOSNAG. DDEC charges[78,79] for the La nodes are of similar magnitude (1.942 |e| in the JOSNAG_clean structure taken directly from the CoRE-MOF database, and 1.902 |e| in the DFT-optimized JOSNAG_clean structure). Thus, complete activation of this MOF involving removal of hydration water bound to the La nodes may prove challenging. In fact, the original synthesis paper pertaining to JOSNAG structure reports a partially dehydrated form of JOSNAG ($[La_2(ad)_3(H_2O)_2]_n$) to have very low surface area (8 m^2/g).[80] However, more recently, new activation methods have been introduced which can greatly improve the pore volume and surface area of the structures as they can prevent structural collapse.[81] Thus, we believe that revisiting activation of JOSNAG with these new methods bears potential as it can result in a highly porous material providing new opportunities for biogas purification.

There are some limitations to the type of high-throughput screening carried out in this work. Although generic force fields allow for expediently predicting the adsorption in materials with diverse chemical nature, it has been shown earlier that the generic force fields may fail to describe the adsorbate-framework interactions accurately for the systems with not only open metal sites but also closed metal sites.[71,82] Tailored force fields or first principles simulations

would be needed for materials with very strong guest-host interactions. Similarly, treating the MOF structures as rigid is an approximation made for computational efficiency. There have been numerous previous works where it has been shown that utilizing rigid framework structures in GCMC simulations can lead to satisfactory agreement with experiments.[82–84] However, the extent of MOF flexibility can vary widely depending on the MOF framework and, for some systems, the framework flexibility can result in considerable differences in the adsorption/separation properties.[85] As it has been shown by hybrid Monte Carlo/Molecular Dynamics simulations[86,87], when the flexibility of the frameworks is accounted for, different pore characteristics can also be observed with/without the presence of adsorbate in the pores. Developing tailored force fields and/or accounting for structural flexibility in all parts of the screening would very significantly add to the computational expense.

The aim of this work is to determine candidate MOFs that are more likely to be effective for biogas purification rather than to identify the most optimal MOFs. Our candidate MOF suggestions should be seen as a guidance for further experimental and/or theoretical work to accelerate materials discovery by focusing on a shortlist of materials among thousands of candidates.

Finally, it should be noted that although, in this study, water is not involved in the biogas mixture, water can be present at small concentrations in actual biogas mixtures. Water can interact strongly with the framework through hydrogen bonding or through chemisorption with undercoordinated metal modes and compete against the other contaminants. Thus, its potential presence in the biogas mixture may lead to considerable decrease in the separation performance. It has been recently reported by Fetisov et al.[74] and Daglar et al.[88] that, in the case of CO_2/N_2 separation, the presence of water even at low concentration can significantly lower the CO_2 capacity and/or the CO_2/N_2 selectivity of MOFs.

4 Conclusion

Biogas, already produced at enormous volumes, is an important alternative energy resource but it requires refining (removal of toxic contaminants and of non-combustible CO_2) to obtain high purity biomethane. In this study, the separation performance of metal-organic frameworks made available through the CoRE-MOF database is investigated through a hierarchical screening approach involving pore-size characteristics, simulations of binary and, subsequently, of five-component ($CH_4/CO_2/N_2/H_2S/NH_3$) mixtures. Utilizing the results from GCMC simulations for the more realistic, five-component biogas mixture, a few metrics are determined to assess the performance of materials. The top-performing candidate materials (ZUQVOW_charged, WASTUG_clean, and JOSNAG_clean) are identified by intersecting the list of the top-ranking materials based on the three performance criteria. These MOFs have relatively high selectivities, especially for NH_3, but also for CO_2 and H_2S. However, none of these can effectively capture all contaminants except N_2. However, the three MOFs adsorb NH_3 strongly even at low pressures and, hence, suffer from low NH_3 regenerability. The H_2S working capacity of JOSNAG_clean is also relatively low. Since the ZUQVOW_charged structure found in the CoRE-MOF database

has different moieties than the experimentally reported ones, it is removed from further consideration. As WASTUG_clean structure lacks hydrogen atoms on bridging oxygens, it has also been omitted during the final evaluation of the top performing structures. However, the optimized structure for JOSNAG_clean is mechanically stable and similar in pore characteristics to the structures found in the CoRE-MOF database, but involves complete removal of the hydration water including those bound to La nodes. While at the time JOSNAG was first reported, its partially dehydrated form did not possess a considerable porous nature, the advent of new activation methods may enable the successful dehydration of JOSNAG. Thus, JOSNAG_clean is identified as a promising candidate to be considered for the biogas upgrading.

Conflicts of interest

There are no conflicts to declare.

Acknowledgments

This research is supported by the U.S. Department of Energy, Office of Basic Energy Sciences, Division of Chemical Sciences, Geosciences and Biosciences under Award DE-FG02-17ER16362. Computer resources were provided through this DOE award and also by the Minnesota Supercomputing Institute at the University of Minnesota.

Supporting Information

Selectivity, working capacity, regenerability, pore characteristics; ranking of 40 CoRE-MOF structures for which loadings of the five-component mixture were determined with sufficient precision, and binary GCMC and five-component GCMC results for several selected MOFs.

References

1 N. N. A. N. Yusuf, S. K. Kamarudin and Z. Yaakub, *Energy Convers. Manag.*, 2011, **52**, 2741–2751.

2 T. Remy, E. Gobechiya, D. Danaci, S. A. Peter, P. Xiao, L. Van Tendeloo, S. Couck, J. Shang, C. E. A. Kirschhock, R. K. Singh, J. A. Martens, G. V Baron, P. A. Webley and J. F. M. Denayer, *RSC Adv.*, 2014, **4**, 62511–62524.

3 T. Montanari, E. Finocchio, E. Salvatore, G. Garuti, A. Giordano, C. Pistarino and G. Busca, *Energy*, 2011, **36**, 314–319.

4 Z.-M. Xia, X.-S. Li, Z.-Y. Chen, G. Li, K.-F. Yan, C.-G. Xu, Q.-N. Lv and J. Cai, *Appl. Energy*, 2016, **162**, 1153–1159.

5 L. Lombardia, A. Corti, E. Carnevale, R. Baciocchi and D. Zingaretti, *Energy Procedia*, 2011, **4**, 465–472.

6 C. A. Grande and A. E. Rodrigues, *Ind. Eng. Chem. Res.*, 2007, **46**, 4595–4605.

7 N. Tippayawong and P. Thanompongchart, *Energy*, 2010, **35**, 4531–4535.

8 L. F. Gomez, R. Zacharia, P. Bénard and R. Chahine, *Adsorption*, 2015, **21**, 433–443.

9 B. Yuan, X. Wu, Y. Chen, J. Huang, H. Luo and S. Deng, *Environ. Sci. Technol.*, 2013, **47**, 5474–5480.

10 L. Sigot, M. Fontseré Obis, H. Benbelkacem, P. Germain and G. Ducom, *Int. J. Hydrogen Energy*, 2016, **41**, 18533–18541.

11 P. M. Bhatt, Y. Belmabkhout, A. H. Assen, Ł. J. Weseliński, H. Jiang, A. Cadiau, D.-X. Xue and M. Eddaoudi, *Chem. Eng. J.*, 2017, **324**, 392–396.

12 J. F. Van Humbeck, T. M. McDonald, X. Jing, B. M. Wiers, G. Zhu and J. R. Long, *J. Am. Chem. Soc.*, 2014, **136**, 2432–2440.

13 J. Yang, R. Krishna, J. Li and J. Li, *Microporous Mesoporous Mater.*, 2014, **184**, 21–27.

14 A. C. Elwell, N. H. Elsayed, J. N. Kuhn and B. Joseph, *Waste Manag.*, 2018, **73**, 189–196.

15 S. A. Peter, G. V Baron, J. Gascon, F. Kapteijn and J. F. M. Denayer, *Adsorption*, 2013, **19**, 1235–1244.

16 S. Xiang, Y. He, Z. Zhang, H. Wu, W. Zhou, R. Krishna and B. Chen, *Nat. Commun.*, 2012, **3**, 954.

17 B. Yuan, X. Wu, Y. Chen, J. Huang, H. Luo and S. Deng, *J. Colloid Interface Sci.*, 2013, **394**, 445–450.

18 S. Cavenati, C. A. Grande and A. E. Rodrigues, *Energy & Fuels*, 2006, **20**, 2648–2659.

19 N. B. K. Magnowski, A. M. Avila, C. C. H. Lin, M. Shi and S. M. Kuznicki, *Chem. Eng. Sci.*, 2011, **66**, 1697–1701.

20 J. A. Delgado, M. A. Uguina, J. L. Sotelo, B. Ruíz and J. M. Gómez, *Adsorption*, 2006,

12, 5–18.

21 M.-B. Kim, Y.-S. Bae, D.-K. Choi and C.-H. Lee, *Ind. Eng. Chem. Res.*, 2006, **45**, 5050–5058.

22 M. Mofarahi and F. Gholipour, *Microporous Mesoporous Mater.*, 2014, **200**, 1–10.

23 S. Cavenati, C. A. Grande and A. E. Rodrigues, *J. Chem. Eng. Data*, 2004, **49**, 1095–1101.

24 M. P. S. Santos, C. A. Grande and A. E. Rodrigues, *Ind. Eng. Chem. Res.*, 2011, **50**, 974–985.

25 Y. Jiang, J. Ling, P. Xiao, Y. He, Q. Zhao, Z. Chu, Y. Liu, Z. Li and P. A. Webley, *Chem. Eng. J.*, 2018, **334**, 2593–2602.

26 S. Horike, S. Shimomura and S. Kitagawa, *Nat. Chem.*, 2009, **1**, 695.

27 Z. Wang and S. M. Cohen, *Chem. Soc. Rev.*, 2009, **38**, 1315–1329.

28 O. K. Farha, A. Özgür Yazaydın, I. Eryazici, C. D. Malliakas, B. G. Hauser, M. G. Kanatzidis, S. T. Nguyen, R. Q. Snurr and J. T. Hupp, *Nat. Chem.*, 2010, **2**, 944.

29 C. E. Wilmer, M. Leaf, C. Y. Lee, O. K. Farha, B. G. Hauser, J. T. Hupp and R. Q. Snurr, *Nat. Chem.*, 2012, **4**, 83–89.

30 C. R. Groom, I. J. Bruno, M. P. Lightfoot and S. C. Ward, *Acta Crystallogr. Sect. B*, 2016, **72**, 171–179.

31 Y. G. Chung, J. Camp, M. Haranczyk, B. J. Sikora, W. Bury, V. Krungleviciute, T. Yildirim, O. K. Farha, D. S. Sholl and R. Q. Snurr, *Chem. Mater.*, 2014, **26**, 6185–6192.

32 L. J. Murray, M. Dinca and J. R. Long, *Chem. Soc. Rev.*, 2009, **38**, 1294–1314.

33 A. R. Millward and O. M. Yaghi, *J. Am. Chem. Soc.*, 2005, **127**, 17998–17999.

34 R. J. Kuppler, D. J. Timmons, Q.-R. Fang, J.-R. Li, T. A. Makal, M. D. Young, D. Yuan, D. Zhao, W. Zhuang and H.-C. Zhou, *Coord. Chem. Rev.*, 2009, **253**, 3042–3066.

35 J. S. Seo, D. Whang, H. Lee, S. I. Jun, J. Oh, Y. J. Jeon and K. Kim, *Nature*, 2000, **404**, 982.

36 H. Furukawa, K. E. Cordova, M. O'Keeffe and O. M. Yaghi, *Science.*

37 M. Yoon, R. Srirambalaji and K. Kim, *Chem. Rev.*, 2012, **112**, 1196–1231.

38 L. E. Kreno, K. Leong, O. K. Farha, M. Allendorf, R. P. Van Duyne and J. T. Hupp, *Chem. Rev.*, 2012, **112**, 1105–1125.

39 B. Chen, S. Xiang and G. Qian, *Acc. Chem. Res.*, 2010, **43**, 1115–1124.

40 A. Pal, S. Chand and M. C. Das, *Inorg. Chem.*, 2017, **56**, 13991–13997.

41 A. L. Myers and J. M. Prausnitz, *AIChE J.*, 1965, **11**, 121–127.

42 S. Cavenati, C. A. Grande, A. E. Rodrigues, C. Kiener and U. Müller, *Ind. Eng. Chem.*

Res., 2008, **47**, 6333–6335.

43 A. F. P. Ferreira, A. M. Ribeiro, S. Kulaç and A. E. Rodrigues, *Chem. Eng. Sci.*, 2015, **124**, 79–95.

44 P. Nugent, Y. Belmabkhout, S. D. Burd, A. J. Cairns, R. Luebke, K. Forrest, T. Pham, S. Ma, B. Space, L. Wojtas, M. Eddaoudi and M. J. Zaworotko, *Nature*, 2013, **495**, 80.

45 C. E. Wilmer, O. K. Farha, Y.-S. Bae, J. T. Hupp and R. Q. Snurr, *Energy Environ. Sci.*, 2012, **5**, 9849–9856.

46 N. H. Alsmail, M. Suyetin, Y. Yan, R. Cabot, C. P. Krap, J. Lü, T. L. Easun, E. Bichoutskaia, W. Lewis, A. J. Blake and M. Schröder, *Chem. - A Eur. J.*, 2014, **20**, 7317–7324.

47 Z. Zhang, Z. Li and J. Li, *Langmuir*, 2012, **28**, 12122–12133.

48 D. Damasceno Borges, P. Normand, A. Permiakova, R. Babarao, N. Heymans, D. S. Galvao, C. Serre, G. De Weireld and G. Maurin, *J. Phys. Chem. C*, 2017, **121**, 26822–26832.

49 Y.-S. Bae, K. L. Mulfort, H. Frost, P. Ryan, S. Punnathanam, L. J. Broadbelt, J. T. Hupp and R. Q. Snurr, *Langmuir*, 2008, **24**, 8592–8598.

50 M. S. Shah, M. Tsapatsis and J. I. Siepmann, *Angew. Chemie*, 2016, **128**, 6042–6046.

51 Y. G. Chung, P. Bai, M. Haranczyk, K. T. Leperi, P. Li, H. Zhang, T. C. Wang, T. Duerinck, F. You, J. T. Hupp, O. K. Farha, J. I. Siepmann and R. Q. Snurr, *Chem. Mater.*, 2017, **29**, 6315–6328.

52 E. Haldoupis, S. Nair and D. S. Sholl, *J. Am. Chem. Soc.*, 2010, **132**, 7528–7539.

53 B. J. Sikora, C. E. Wilmer, M. L. Greenfield and R. Q. Snurr, *Chem. Sci.*, 2012, **3**, 2217–2223.

54 E. Haldoupis, S. Nair and D. S. Sholl, *J. Am. Chem. Soc.*, 2012, **134**, 4313–4323.

55 E. Haldoupis, S. Nair and D. S. Sholl, *Phys. Chem. Chem. Phys.*, 2011, **13**, 5053–5060.

56 T. F. Willems, C. H. Rycroft, M. Kazi, J. C. Meza and M. Haranczyk, *Microporous Mesoporous Mater.*, 2012, **149**, 134–141.

57 D. Ongari, P. G. Boyd, S. Barthel, M. Witman, M. Haranczyk and B. Smit, *Langmuir*, 2017, **33**, 14529–14538.

58 C. E. Wilmer, K. C. Kim and R. Q. Snurr, *J. Phys. Chem. Lett.*, 2012, **3**, 2506–2511.

59 Y. Sun, R. F. DeJaco and J. I. Siepmann, *Chem. Sci.*, 2019, **10**, 4377–4388.

60 D. Dubbeldam, S. Calero, D. E. Ellis and R. Q. Snurr, *Mol. Simul.*, 2016, **42**, 81–101.

61 A. K. Rappe, C. J. Casewit, K. S. Colwell, W. A. Goddard and W. M. Skiff, *J. Am. Chem. Soc.*, 1992, **114**, 10024–10035.

62 M. G. Martin and J. I. Siepmann, *J. Phys. Chem. B*, 1998, **102**, 2569–2577.

63 J. J. Potoff and J. I. Siepmann, *AIChE J.*, 2001, **47**, 1676–1682.

64 M. S. Shah, M. Tsapatsis and J. I. Siepmann, *J. Phys. Chem. B*, 2015, **119**, 7041–7052.

65 L. Zhang and J. I. Siepmann, *Collect. Czechoslov. Chem. Commun.*, 2010, **75**, 577–591.

66 G. Kresse and J. Furthmüller, *Phys. Rev. B*, 1996, **54**, 11169–11186.

67 P. E. Blöchl, *Phys. Rev. B*, 1994, **50**, 17953–17979.

68 J. P. Perdew, K. Burke and M. Ernzerhof, *Phys. Rev. Lett.*, 1996, **77**, 3865–3868.

69 S. Grimme, J. Antony, S. Ehrlich and H. Krieg, *J. Chem. Phys.*, 2010, **132**, 154104.

70 S. Grimme, S. Ehrlich and L. Goerigk, *J. Comput. Chem.*, 2011, **32**, 1456–1465.

71 A. L. Dzubak, L.-C. Lin, J. Kim, J. A. Swisher, R. Poloni, S. N. Maximoff, B. Smit and L. Gagliardi, *Nat Chem*, 2012, **4**, 810–816.

72 E. Haldoupis, J. Borycz, H. Shi, K. D. Vogiatzis, P. Bai, W. L. Queen, L. Gagliardi and J. I. Siepmann, *J. Phys. Chem. C*, 2015, **119**, 16058–16071.

73 H. Fang, H. Demir, P. Kamakoti and D. S. Sholl, *J. Mater. Chem. A*, 2014, **2**, 274–291.

74 E. O. Fetisov, M. S. Shah, J. R. Long, M. Tsapatsis and J. I. Siepmann, *Chem. Commun.*, 2018, **54**, 10816–10819.

75 Z. Qiao, C. Peng, J. Zhou and J. Jiang, *J. Mater. Chem. A*, 2016, **4**, 15904–15912.

76 K. Lee, W. C. Isley, A. L. Dzubak, P. Verma, S. J. Stoneburner, L.-C. Lin, J. D. Howe, E. D. Bloch, D. A. Reed, M. R. Hudson, C. M. Brown, J. R. Long, J. B. Neaton, B. Smit, C. J. Cramer, D. G. Truhlar and L. Gagliardi, *J. Am. Chem. Soc.*, 2014, **136**, 698–704.

77 P. Bai, M. Y. Jeon, L. Ren, C. Knight, M. W. Deem, M. Tsapatsis and J. I. Siepmann, *Nat. Commun.*, 2015, **6**, 5912.

78 T. A. Manz and N. G. Limas, *RSC Adv.*, 2016, **6**, 47771–47801.

79 N. G. Limas and T. A. Manz, *RSC Adv.*, 2016, **6**, 45727–45747.

80 V. Kiritsis, A. Michaelides, S. Skoulika, S. Golhen and L. Ouahab, *Inorg. Chem.*, 1998, **37**, 3407–3410.

81 J. Ma, A. P. Kalenak, A. G. Wong-Foy and A. J. Matzger, *Angew. Chemie Int. Ed.*, 2017, **56**, 14618–14621.

82 H. Demir, J. A. Greathouse, C. L. Staiger, J. J. Perry IV, M. D. Allendorf and D. S. Sholl, *J. Mater. Chem. A*, 2015, **3**, 23539–23548.

83 M. Agrawal and D. S. Sholl, *ACS Appl. Mater. Interfaces*, 2019, **11**, 31060–31068.

84 J. Park, J. D. Howe and D. S. Sholl, *Chem. Mater.*, 2017, **29**, 10487–10495.

85 J. A. Gee and D. S. Sholl, *J. Phys. Chem. C*, 2016, **120**, 370–376.

86 S. M. J. Rogge, R. Goeminne, R. Demuynck, J. J. Gutiérrez-Sevillano, S. Vandenbrande,

L. Vanduyfhuys, M. Waroquier, T. Verstraelen and V. Van Speybroeck, *Adv. Theory Simulations*, , DOI:10.1002/adts.201800177.

87 M. V Parkes, H. Demir, S. L. Teich-McGoldrick, D. S. Sholl, J. A. Greathouse and M. D. Allendorf, *Microporous Mesoporous Mater.*, 2014, **194**, 190–199.

88 H. Daglar and S. Keskin, *J. Phys. Chem. C*, 2018, **122**, 17347–17357.

TOC Graphic

A hierarchical screening process is used to find a potentially top-performing metal-organic framework for biogas purification.

TOC Graphic and Text

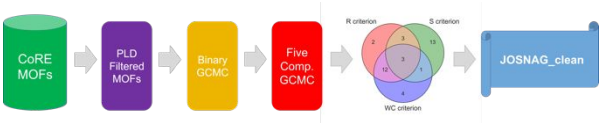

A hierarchical screening process is used to find a potentially top-performing metal-organic framework for biogas purification.